Solid Freeform Fabrication 2016: Proceedings of the 27th Annual International Solid Freeform Fabrication Symposium – An Additive Manufacturing Conference
Reviewed Paper

INFLUENCE OF EMBEDDING PROCESS ON MECHANICAL PROPERTIES OF MATERIAL EXTRUSION PARTS

Swapnil Sinha and Nicholas A. Meisel
Made By Design Laboratory
School of Engineering Design, Technology, and Professional Programs, Penn State

ABSTRACT

The layer-by- layer deposition of material in Additive Manufacturing (AM) introduces the capability for in-situ embedding of functional components into printed parts. The typical embedding process involves, i) designing the cavity for the embedded component, ii) pausing the print when the top layer of the cavity is reached, iii) manually inserting the component, and iv) resuming the build process. However, the effect of different interfacial materials (due to the presence or absence of a shape converter) and the pause time during the build process on a part's material properties is not well-understood. Therefore, the tensile strength of 3D-printed embedded specimens with and without shape converters and with different intervals of pause time is tested in this study. The results from this experimental analysis can be useful for the design guidelines for AM with embedded components as they provide an initial understanding of mechanical properties of these parts.

1. INTRODUCTION

Moving from rapid prototyping towards direct manufacturing, additive manufacturing (AM, also known as 3D printing) has evolved as a manufacturing method over the past thirty years, offering unparalleled capability in terms of accessibility of technology, flexibility of design, and creation of end-use products [1]. As an inexpensive and relatively uncomplicated process, material extrusion or fused deposition modelling (FDM) is one of the most common and widely used types of AM. In material extrusion, a heated nozzle melts, extrudes, and deposits the fed thermoplastic filament on a build tray in a prescribed geometry. Solid layers are generated by side-by-side deposition and solidification of molten roads of thermoplastic. The build tray is lowered once a layer is completed. The next layer bonds with the previous layer as it cools down. The control of thermal environment is important for successful bonding of roads, and hence the system is often enclosed to maintain appropriate temperature below the melting point of the material being extruded [2].

Contrary to traditional subtractive manufacturing, the layer-by-layer nature of AM allows for access to the entire volume of the workpiece throughout the build process. This, in turn, gives an opportunity to embed sensors, actuators, circuits, and other functional components within a part during the manufacturing process [3,4]. Its applications have recently been recognized for design and production of optimized parts and sophisticated "smart" objects. Typically, the embedding process in AM involves 1) designing the cavity for the embedded component, 2) pausing the print when the top layer of the cavity is reached, 3) inserting the component and 4) resuming the printing process [4]. While in-situ embedding is a powerful tool for AM, there are two factors that may greatly affect the strength of these embedded parts: process interruption and material transition. Since thermal environment control is crucial for bonding [2], an interruption in the process causes the layer to cool down, and may affect the layer bonding when resumed. The material transition

occurs when the printing is resumed after embedding a foreign component. The cavity is covered with another component and the resumed layer is deposited on it. While qualitative observation notes that the layer adhesion may be impacted by both of these factors, their effects on the overall strength of the part are unknown.

In this research paper, the effects of the embedding process on the strength of material extruded parts were studied by preparing specimens with a Mark One 3D printer. The Mark One printer by MarkForged is a 3D printer capable of creating carbon fiber reinforced thermoplastic parts via dual-extrusion of a Nylon base material with continuous carbon fibers. This combination of polymer printing with continuous carbon fibers enables users to create physical objects with high strength to weight ratios; the carbon fiber prints are claimed to be twenty times stiffer and five times stronger than standard ABS plastic [5], making it practical to produce high strength parts with AM. With the printer, users can also preselect a layer and insert a pause while preparing the 3D model for printing. The print bed reregisters with 10-micron accuracy, allowing users to pause a print, remove the bed, add components, reinsert the bed, and then continue the print with a high degree of precision. This focus on the potential of in-situ embedding in AM gives the Mark One an advantage over similar desktop material extrusion systems, and makes it a well-poised candidate for study of the impacts of in-situ embedding within AM.

2. LITERATURE REVIEW

Previous research related to embedding with AM has been divided into three parts. Section 2.1 explores the diverse applications of the embedding process. Section 2.2 summarizes prior efforts in embedding materials using different AM process types. Section 2.3 outlines the research on mechanical properties of embedded parts. This includes considerations for designing embedded components and addresses concerns with mechanical properties of embedded parts.

2.1 Multi-Functional parts via AM

The popularity of the Internet of Things [6] has spurred recent AM research in the validation of both form with functionality, which primarily involves embedding functional components in parts [7–10]. Technologies such as near field communication, real-time localization, and feedback from embedded sensors has enabled the transformation of everyday objects into smart objects. These objects are aware of their surroundings and can communicate or react accordingly[11,12]. Isanaka and co-authors summarized these roles of embedding via AM technologies to help establish a Cyber-Enabled Manufacturing (CEM) environment. The CEM environment is a smart manufacturing environment, which consists of a network of embedded sensors, coupled with control systems, to effectively gather information and offer immediate response in manufacturing facilities [13]. AM makes embedding these sensors feasible and accessible. Integrating current technologies with AM allows for the design and production of sophisticated products in a CEM-like automated manner, and therefore with reduced product development cycle time [7,14].

One of the major applications of multi-functionality is structural health monitoring (SHM), which is an emerging method for non-destructive product evaluation. It requires sensors to be embedded into the structure to capture, log, and analyze real time data about the health of the structure. Benefits of this application are realized in structures like bridges, buildings, aircrafts and mega machines where catastrophic failures must be avoided [15]. Strantza and co-authors [16]

evaluated the performance of SHM systems embedded via AM, for their suitability in non-destructive testing of structures. The system was found reliable, and is expected to be used to obtain a novel approach to structural design that relies on lightweight structures. This rise in applications of in-situ embedding via AM in the fields requiring high safety and performance standards, require careful process and quality control. Suitable standards for testing will ensure the acceptance of this rising technology [1].

2.2 Embedding in different AM process types

Layer by layer material addition allows for in situ embedding applications to be realized in a wide variety of AM process types. A significant amount of the research on embedding via AM has been done with Stereolithography (SLA) process, a vat photo-polymerization AM technology [9]. Kataria and Rosen [17] demonstrated methods for fabricating embedded complex devices in SLA. Macdonald and co-authors [7] developed an SLA process to 3D print electronics, in order to reduce product development cycle time. SLA has also been used to fabricate 3D printed structures with embedded electronics for a space vehicle 'CubesSat Trailblazer', launched by NASA in November 2013. However, a lack of durability was identified due to the material properties of the photopolymer resin, which is the material used for fabrication in SLA process [14,18].

When considering embedding within metal structures, traditional powder metallurgy processes involve isostatic pressing and diffusion bonding and are capable of reaching a temperature up to 565°C. This high temperature can prove damaging for sensitive embedded components, which has limited its usefulness in embedding applications [19]. In the area of metal powder-bed fusion AM, Rodriguez and coauthors [20] measured the surface temperature while printing through electron beam melting process by embedding a thermocouple in the build plate. The electron beam can make the temperature of the metal surface to go up to 2269°C [21], making it impossible to insert overly delicate components. The sheet lamination process, ultrasonic additive manufacturing (UAM) is a solid state joining process in which thin metallic tapes are ultrasonically welded on top of one another and periodically machined to create a final part [22]. Hahnlel and co-authors demonstrated a successful electrical insulation of embedded material through UAM process on aluminum matrix composites. The parts fabricated through this process experience temperature as low as 25°C and therefore it is safe for embedded components like smart materials or sensors [19]. However, UAM has limited success bonding dissimilar materials, limiting its application in the aerospace, automotive, electrical and power generation industries [23].

The material jetting process is an AM technique that utilizes drop-on-demand inkjet printing to selectively deposit droplets of photopolymer directly onto a build platform. Because of low range of working temperature and direct material addition layer after layer, this process has proven well-suited for component embedding. However, the print head assembly block passes over the printed part at a clearance of only 100 microns. Any protrusions from the embedded component can cause damage to the nozzle [4]. Also, there is only a limited number of photo polymeric materials available for material jetting. As with SLA, this type of material results in fragile parts.

Polymer material extrusion is the one of the least explored but also potentially the most useful AM process types for in-situ embedding. With proper clearance design, components can be embedded without subjecting them to damaging temperature and pressure. While inherent limitations of material extrusion make it difficult to produce high tolerance or products with a fine

surface finish, this limitation can be eliminated by its ability to embed highly finished parts like bearings and shafts [24]. Sbriglia and co-authors [25] embedded sensors in a material extrusion part to analyze the operational choice for the process. The study concurred with the findings of Stark and co-authors about embedding sensors in FDM parts as a useful method for state-of-health monitoring in deployed systems [26]. Aguilera and co-authors also demonstrated an integrated process for embedding high performance conductors directly into the thermoplastic material extrusion substrate [27]. The wide variety of hybrid processes and thermoplastics available for material extrusion help to enable its wide application in various industries and make it a suitable candidate for in-situ embedding research.

2.3 Mechanical Properties of Embedded Parts

Because inter-layer bond strength is a major factor when it comes to the mechanical properties of 3D printed part [28], in-situ embedding has the likely potential to impact a structure's mechanical properties. However, a review of the available literature shows that research in this area is still sparse. Klift, Koga, Todoroki, Ueda, & Hirano, performed tensile tests using Mark One 3D printer to compare strength differences in two layered (2CF) and six layered (6CF) continuous carbon fiber embedded within a Nylon base. The tests revealed that discontinuities of the fibers led to premature failure in the areas where fibers were absent and reduced the tensile strength of the composite material. A further investigation of cross sections of 2CF and 6CF specimens revealed that there was more void area in 6CF specimens. These voids had a negative impact on the elastic modulus of the composite, which calls for future work on effects of different arrangements of carbon fiber layers on the mechanical properties of these composites [29]. Outside of AM, a study on mechanical properties of casted epoxy resin with and without embedded silicon substrates verified that the ultimate tensile strength dramatically reduced in comparison to that of without embedding. Also, the points of failure for each specimen were located on the embedded section. It was concluded that the strength of the part embedded with an insert will have to be investigated if the insert is harder [30].

2.4 Context

As this review shows, existing literature has demonstrated a consistent growth in acknowledgement of applications of embedding via AM. This has led to further investigations into processes which could assist in embedding. However, to the best of the author's knowledge, there is little-to-no research performed to understand the effects of process interruption or embedding on the properties of the printed parts. To address this critical gap, the purpose of this paper is to investigate the effects of the embedding process on the mechanical properties of material extrusion parts. To this end, the authors use tensile testing in order to determine i) how process interruption affects the strength of a printed part and ii) how the presence of an embedded artifact affects the strength of the printed part. Process interruption specimens are prepared carefully with different pause time intervals, to test if there is any correlation between print pause interval and mechanical properties, while embedding specimens include both those with shape converters and without shape converters. Knowledge of the influence of these parameters can greatly benefit in making design decisions for manufacturing systems or for preparing safety critical parts. Section 3 of this paper discusses the experiment performed to findings on effects of process interruption on strengths of the parts. Section 4 discusses the effects of embedding process found through experimentation on the strength of the parts. Section 5 summarizes the findings of this research paper and discusses the gaps and future work in order.

3. EFFECTS OF PROCESS INTERRUPTION

3.1 Experimental Setup

Process interruption during printing is a requirement while embedding, but these interruptions can also be caused by power outages, system errors or material shortages. When dealing with such issues, the decision of whether to resume the print or to restart the print, lies with the system user. To make an informed decision, it is necessary to know the impact of this interruption on the strength of the printed part. To better understand these effects, a Mark One 3D printer is used to create specimens from nylon filament. The system can achieve a layer resolution of 100 microns and Eiger (Mark Forged's cloud based, print preparation software) gives a provision to insert a pause after any selected layer. This allows for a precise consistency in specimens prepared. All the specimens were printed with z axis orientation (Figure 1) so as to study the magnified effects of process interruption on tensile properties of the parts.

(a) (b)

Figure 1. (a) Build orientation of the specimen on Mark One and (b) Mark One while printing the specimen.

Standard ASTM specimen designs were attempted for print [31], however, the specimen dimensions were either too thin for a successful print (Figure 2a), or too tall to fit within the build volume. After several attempts at specimen design, the final design (Figure 2b and 2c) was selected based on physical limits of the build platform, success of the print, and careful consideration of parameters to be studied. The strength along z- axis is lower for material extrusion parts as compared to other build orientations. This material anisotropy is an inherent limitation of material extrusion process, as material likely cools more thoroughly between layers than between roads, potentially affecting fusion of the thermoplastic [32]. Therefore, specimens prepared in this orientation will be more sensitive to the effects of process interruption. This allows authors to study if the embedding process introduces a weakness on the layer where the pause occurs.

Specimen design for different treatments (no pause and pause with time duration of 5, 15, 30 and 60 minutes) are shown in Figure 2b and 2c. The reference specimens, with 0 minutes of pause time, were designed with the dimension of 12mm x 24mm x 96mm and were printed without any process interruption. For process interruption, specimens were printed with a pause at the center layer using Eiger (as shown in Figure 2c). These specimens were prepared with pause time intervals of 60 minutes, 30 minutes, 15 minutes and 5 minutes.

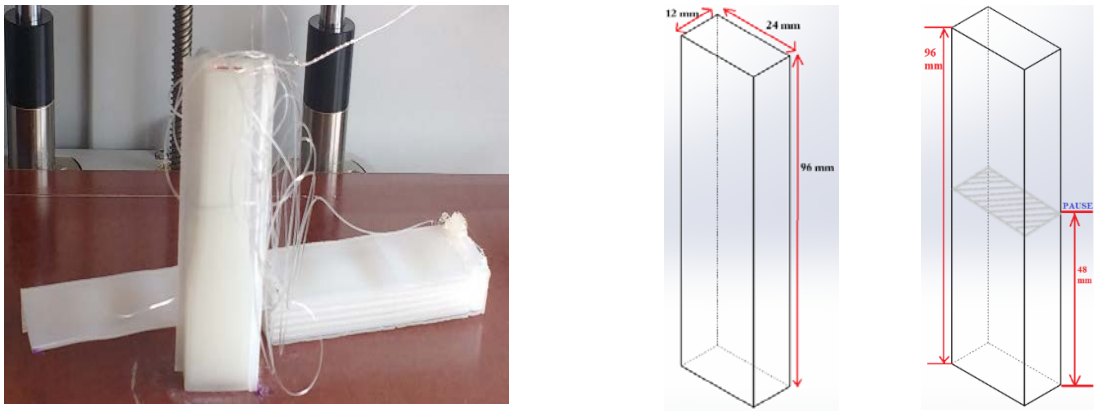

(a) (b) (c)

Figure 2. Shows (a) the failed print of a standard ASTM dogbone sample design, (b) the final design of specimen for no pause and (c) with pause of different time durations.

The build was prepared using the Eiger software with 0.2 mm layer height, 100% fill density, and rectangular fill pattern. Each specimen was printed individually and stored in a dark location at room temperature (24°C), with 50% humidity. Desiccant packets were used in an attempt to control the impact of humidity. The testing was performed after at least 48 hours of storage. The final printed specimens are shown in Figure 3.

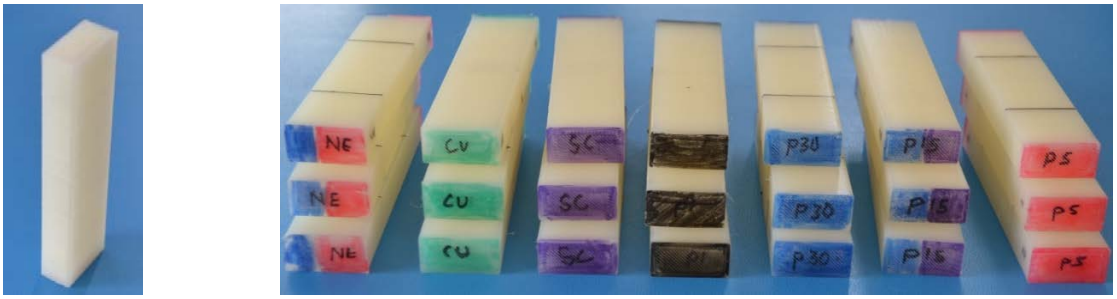

(a) (b)

Figure 3. (a) A single printed specimen for tensile testing and (b) all specimens prepared and marked for indicating treatments, before tensile testing.

Tensile testing was performed using Instron 5866 Mechanical Testing Machine, using mechanical wedge action grips on a 5kN load cell (Figure 4). The pull rate was 5mm/min. Serrated jaw faced grips of thickness range 6.35mm to 12.7mm were used. Gauge length, width, and thickness of each samples were recorded in millimeters and every 0.1 second the extension (mm), tensile stress (MPa), load (N), and tensile strain (mm/mm) were recorded. The temperature during testing was recorded as 24°C and the humidity was recorded as 55%.

Figure 4. Tensile testing on Instron 5866 Mechanical Testing Machine.

3.2 Results and discussion

The statistics of the maximum tensile stress data obtained are reported in Table 1. Three specimens were tested for each treatment.

Table 1. Statistics of maximum tensile stress (MPa) values obtained for each treatment:

Treatment	*Mean*	*Median*	*Std. Deviation*	*Variance*	*Range*	*Minimum*	*Maximum*
0 minute pause	13.03	12.92	0.202	0.04	0.36	12.90	13.26
5 minute pause	7.43	7.90	1.42	2.01	2.72	5.84	8.56
15 minute pause	7.00	7.03	0.75	0.57	1.51	6.23	7.740
30 minute pause	6.27	6.13	0.69	0.48	1.36	5.66	7.02
60 minute pause	7.54	7.17	0.75	0.56	1.35	7.05	8.40

To perform statistical analysis on the data obtained so as to find the significance in the differences recorded, the data was checked for the assumptions for parametric testing. These were, independence of cases, normality, and homogeneity of variances. All the assumptions were met except for normality. The Shapiro-Wilk test (Table 2) confirmed that the data for Maximum Tensile Stress is not normal ($p=0.002, < 0.05$). Therefore, non-parametric tests were performed to analyze data for maximum tensile stress.

Table 2. Tests for Normality

	Kolmogorov-Smirnov[a]			**Shapiro-Wilk**		
	Statistic	*df*	*Sig.*	*Statistic*	*df*	*Sig.*
Maximum_Tensile_Stress	.254	15	.010	.786	15	.002

a. Lilliefors Significance Correction

Since there are five groups (treatments) to be compared, a Kruskal-Wallis H test (also known as one-way ANOVA on ranks) was performed to identify if there was any statistically significant difference in the data due to treatments. A Kruskal-Wallis H test is a rank-based nonparametric test used to determine if there are statistically significant differences between two or more groups of an independent variable on a continuous or ordinal dependent variable. The test showed that there was a statistically significant difference in Maximum Tensile stress values

between different treatments, $\chi 2(2) = 9.633$, p=0.047, with a mean rank of 14.00 for no pause, 8.00 for 5 minutes pause, 6.33 for 15 mins pause, 3.00 for 30 mins pause and 8.67 for 60 mins pause. Effect size quantifies how well this difference works in a range of contexts. This value can be calculated as shown below, where N is the total number of observations.

$$\text{Effect size} = \chi 2/(N-1)$$
$$= 9.633/(15-1)$$
$$= 0.688$$

The value 0.688 of effect size means that 68.8% of the variability in rank scores is accounted for by different treatments. The Kruskall Wallis test only verifies that at least two groups were significantly different. To identify where these differences occurred, post hoc analysis was performed by pairwise comparision of each combination of groups (based on treatment). To study the individual tensile property effects of process interruption while embedding (pausing the print to insert) or due to system errors, the specimens prepared with pause were compared by grouping them on the basis of time interval of pause. The reference values were set to be the data obtained for specimens with no process interruption (0 minutes pause). The maximum tensile stress values are reported by pause time intervals in Figure 5. Error bars indicate sample standard deviations of the data points for each treatment.

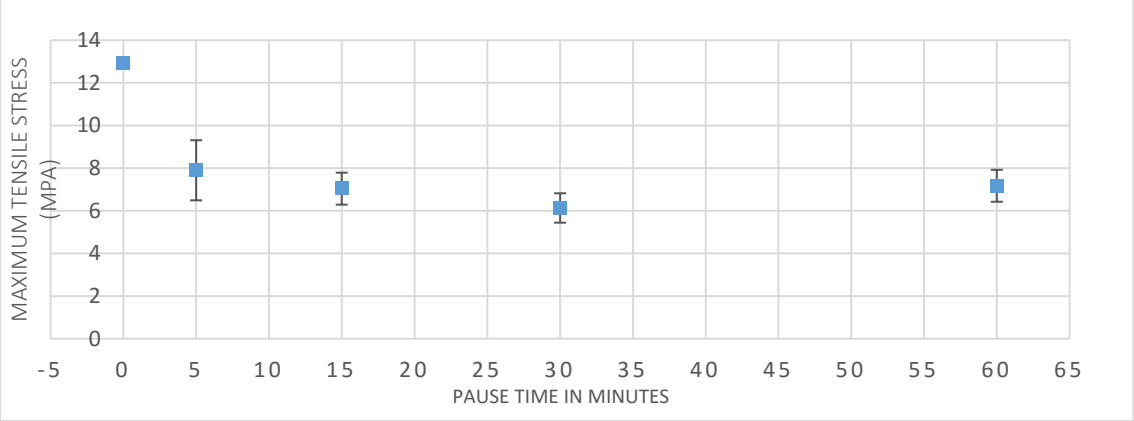

Figure 5. Median values of Maximum tensile stresses of specimens with respect to their pause time

The graph shows a clear difference between maximum tensile stress values of specimens with process interruption (5, 15, 30 and 60 minutes of pause) and specimens without any process interruption (0 minutes of pause). However, there is no clear difference in maximum tensile stress values of specimens with different pause time (>0 minutes).

The post-hoc test performed on the data was the Mann Whitney U test, which is a non parametric test to compare two independent groups. Pairwise U and p values for Mann Whitney U tests are shown in Table 3. Any p-value of 0.05 or less has been highlighted to indicate statistical significance in difference of maximum tensile stress values. This test helps in identifying the differences which are significant, which could not be obtained using the earlier Kruskall Wallis H test.

Table 3. Post Hoc analysis results of pairwise comparison of different pause time treatment.

Treatment	Mann Whitney U test	0 mins |Mdn=12.917	5 mins | Mdn=7.899	15 mins | Mdn=7.037	30 mins | Mdn=6.131	60 mins | Mdn=7.173
0 mins |Mdn=12.917	U	-	0	0	0	0
	p	-	0.05	0.05	0.05	0.05
5 mins | Mdn=7.899	U		-	3	2	4
	p		-	0.35	0.2	0.5
15 mins | Mdn=7.037	U			-	1	2
	p			-	0.1	0.2
30 mins | Mdn=6.131	U				-	0
	p				-	0.05

The Mann-Whitney U test indicated that the ultimate tensile strength was greater for specimens with no pause (Median= 12.917 MPa) than for specimens with 5 minutes pause (Median= 7.899MPa), 15 mins pause (Median= 7.037 MPa), 30 minutes pause (Median= 6.131 MPa), and 60 minutes pause (Median=7.173 MPa). This shows that there is a statistically significant effect of process interruption on the tensile strength of the printed part. Since there is no statistically significant difference in maximum tensile stresses compared pairwise for different pause times (>0 minutes), the statitical analysis suggests that the magnitude of pause time has no significant effect on the strength of the part. However, there is a significant statistical difference between maximum tensile stress values for pause time interval of 30 minutes and that of 60 minutes. This difference is inconsistent with results of other pairs of pause time intervals; more data points are required to confirm the reason for this difference.

Another observation from the tensile testing of specimens was made on the location of failure (Figure 6). The layer of failure for each specimen with process interruption was always the layer which was paused (center layer). The layer of failure for specimens without any process interruption varied across the part. This confirms that process interruption introduces weakness on the layer at which the process was interrupted. This information is important for designing functional components to be manufactured by in situ embedding via AM. The location of embed is advised to be decided by considering the location of layer to be paused.

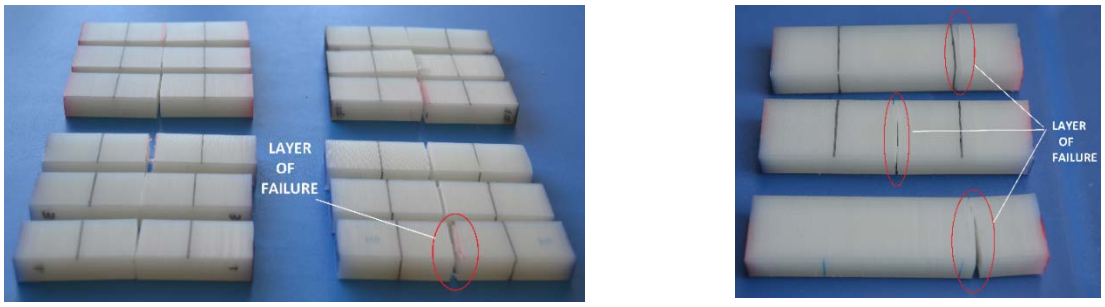

(a) (b)

Figure 6. Examples of specimen failure after testing with (a) process interruption specimens grouped based on time interval for pause, all failed at the layer which was paused, and (b) specimens with no process interruption, failed at varying layers.

3.3 Summary of Key Findings

Tensile testing specimens created to study the effects of process interruption allow the authors to conclude the following:

- The Maximum Tensile stress value decreases significantly because of process interruption. The median tensile strength reduced to as low as 48%
- The Maximum Tensile Stress value has no effect due to time duration of pause ≥ 5 minutes.

The test verifies that the presence of a process interruption, irrespective of time duration ≥ 5 minutes, has a negative impact on tensile strength of the part. For a safety critical part or parts requiring high strength, it is advised that the print shoud be restarted if there is any process interruption.

4. EFFECTS OF EMBEDDING WITH AND WITHOUT SHAPE CONVERTER

For an embedded part via AM, the stress concentrations caused due to the presence of cavity for inserts, are expected to reduce the tensile strength of the part. When embedding a component with an irregular top surface, covering the cavity with a shape converter on the paused layer provides support to the resumed layer. Embedding components with flat surfaces may not require shape converters, however, the layer adhesion may reduce because of material transition between the top surface of the embed and the resumed layer. If the shape converter is of the same material as the print, the authors hypothesize that it should assist in better layer adhesion between paused and resumed layer.

To understand the effects of this material transition in different embedding processes on the strength of the part, specimens were prepared with four different treatments: two different embedding methods (with and without shape converters), process interruption, and without any process interruption. The specimens were printed in z-axis orientation on Mark One 3D printer with nylon filament. Specimens with and without any process interruption were designed and prepared similarly to those in Section 3. The two types of specimens for embedding were designed with cavities as shown in Figure 7. The first type of specimen was designed with a cavity of cross section 5mm x 11mm at the center layer, with a depth of 0.5mm, in order to embed a small piece of copper tape. The copper tape insert was selected because of its applications in direct writing for in situ embedding. Copper tape also offers a smooth surface for the resumed layer. This allows to compare and evaluate the effects of shape converter, when not used for supporting the resumed layer. The cross section of the cavity was decided after multiple print attempts of different cross sections and their success of completion. The second type of embedded specimen was designed in order to embed with a shape converter. This specimen was also designed with a cavity of cross section 5mm x 11mm at the center of the part. The depth of the cavity was selected as 3mm, in order to embed a printable shape converter. The shape converter was designed and printed with the same system, parameters, and material as the specimen.

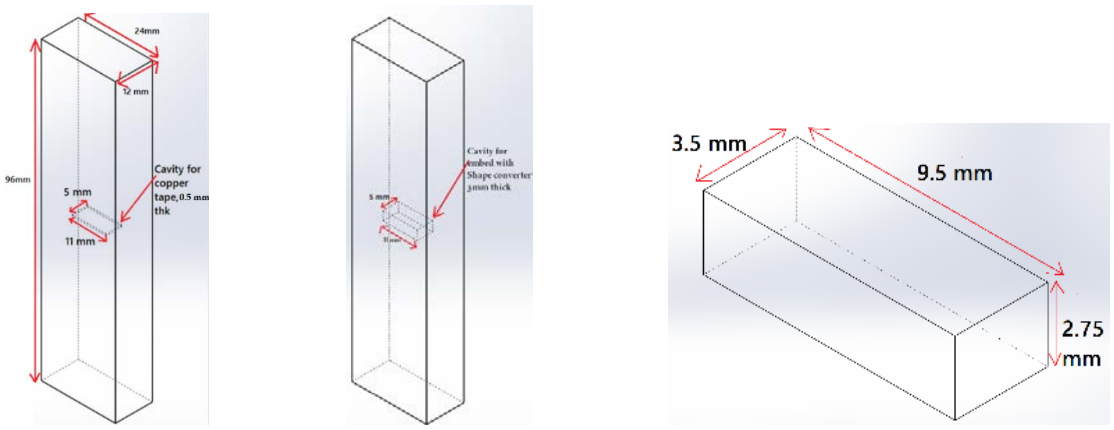

(a) (b) (c)

Figure 7. Specimen design for copper tape embed (a), and shape converter embed (b), with the dimensions of shape converter shown in (c).

To determine the design clearance for the cross section of the shape converter, a set of shape converter with clearance varying from 0mm to 2 mm in both x and y axis of the build were printed. These shape converters were then inserted in the cavity of designed cross section 5mm x 11mm, as shown in Figure 8. As shown in Figure 8b, the shape converter with a design clearance of 1.5mm in both x and y axes was selected as the most suitable dimension of shape converter for embedding. The selection was done on the basis of its ease of fit and low clearance with the walls of the cavity.

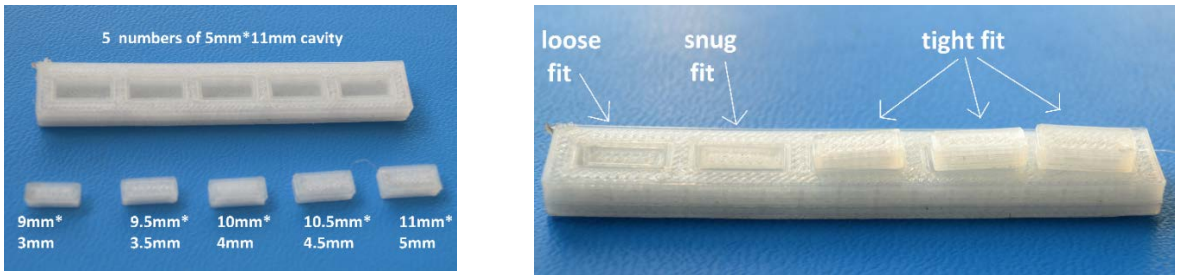

(a) (b)

Figure 8. (a) Initial shape converters with different clearance values varying from 0mm to 2mm in both x and y axis and (b) demonstration that clearance of 1.5mm in both x and y axis was found to fit snuggly in the cavity.

To find the clearance for shape converter in the z-direction, another set of shape converters were prepared with same cross sections (9.5mm x 3.5mm) but with different thicknesses (varying from 2mm to 3mm, as shown in Figure 9a) to find its fit in a cavity designed with 3mm depth. The alignment of the top layer of the shape converter was checked after inserting it in the cavity. As shown in Figure 9b, the shape converter with designed z axis clearance of 0.25mm from the cavity aligned with the top layer, and was selected as appropriate z axis clearance for the shape converter. The cavity due to the indented shape converters would not solve the purpose of inserting a shape converter to improve strength and the protruded shape converter would be damaging for the print head if the print is resumed. The aligned specimen was chosen so as to magnify the effects (if any) of the inter-layer bond strength between the top layer of shape converter and the resumed layer. Therefore, the shape converter was designed with a clearance of 1.5 mm on x and y axis each. The

z axis clearance was made 0.25 mm so that the top plane of the shape converter coincides with the paused layer of the part, after being inserted in the cavity.

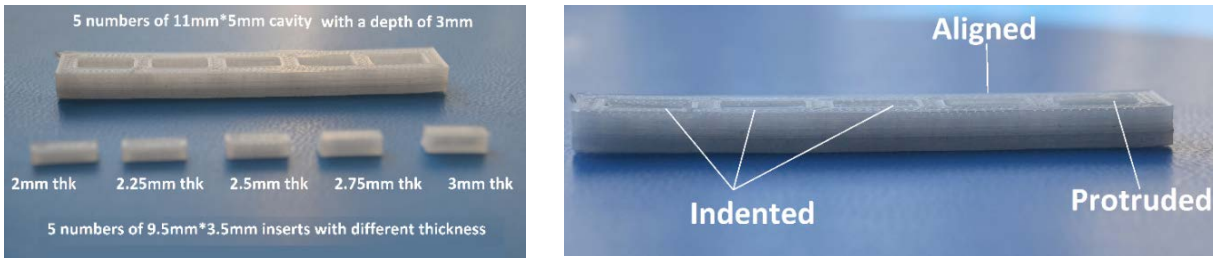

(a) (b)

Figure 9. (a) Initial shape converters of same cross sections but different thicknesses values, varying from 0mm to 1mm and (b) demonstration that the shape converter with a design clearance of 0.25mm in z axis was the most aligned with the top layer.

After the selection of clearance values, the design of the specimens were printed for testing. The printing parameters and testing environment were the same as in Section 3. The printing process was paused for 15 minutes right after the cavity was printed, to embed the copper tape with dimensions 5mm x 11mm, inside the cavity.

4.2 Results and Discussions

The statistics of the data obtained for the maximum tensile stresses of the specimens for each treatment are reported in Table 4.

Table 4. Statistics of data obtained for Maximum Tensile Stress values (MPa) for each treatment:

Treatment	Mean	Median	Std. Deviation	Variance	Range	Minimum	Maximum
No process interruption	13.03	12.92	0.20	0.04	0.36	12.90	13.26
Copper tape embed	5.28	5.12	0.96	0.92	1.90	4.41	6.31
Shape converter embed	5.11	4.97	0.68	0.46	1.34	4.50	5.84
With Process interruption	7.54	7.17	0.75	0.56	1.35	7.05	8.40

The data was checked for the assumptions for parametric testing. Shapiro-Wilk test (Table 5) confirmed that the data for Maximum Tensile Stress is not normal ($p=0.014$, < 0.05). Therefore, non-parametric tests were performed to analyze data for maximum tensile stress.

Table 5. Tests for Normality

	Kolmogorov-Smirnov[a]			Shapiro-Wilk		
	Statistic	df	Sig.	Statistic	df	Sig.
Maximum_Tensile_Stress	.233	12	.071	.815	12	.014

a. Lilliefors Significance Correction

The Kruskall Wallis H test showed that there was a statistically significant difference in Maximum Tensile stress values between different treatments, $\chi 2(2) = 9.359$, $p=0.025$, with a mean rank of 11.00 for no process interruption, 3.67 for copper tape embed, 3.33 for shape converter embed, and 8.00 for specimens with process interruption. Effect size was calculated as below:

$$\text{Effect size} = \chi 2/(N-1)$$
$$= 9.359/(12-1)$$
$$= 0.8508$$

The value 0.8508 of effect size means that about 85% of the variability in rank scores is accounted for, by different treatments. Statistical analysis (Mann Whitney U Test) was performed pairwise on the groups of treatments, to find the significance in difference of maximum tensile stress. Pairwise U and p values for the test are shown in Table 6; any p-value of 0.05 or less has been darkened to signify statistical significance in difference of ultimate tensile stress.

Table 6. Post Hoc analysis results of pairwise comparison of groups with different embedding conditions, only process interruption, and no process interruption.

Condition	Mann Whitney U test	Process Interruption | Mdn=7.044	Copper Tape embed | Mdn=5.121	Shape converter embed | Mdn=4.976
No interruption |Mdn=12.917	U	0	0	0
	p	0.05	0.05	0.05
Process Interruption| Mdn=7.044	U	-	0	0
	p	-	0.05	0.05
Copper tape embed| Mdn=5.121	U		-	4
	p		-	0.827

The Mann Whitney U test indicated that the ultimate tensile strength for specimens with embedding (Copper tape Mdn=5.048 MPa & Shape converter embed Mdn=4.976 MPa) is significantly less than for specimens with just a pause (Mdn= 7.173 MPa), U=0, p=0.05. This can be explained by the presence of cavity in the specimens which were embedded. Theoretically, presence of cavity in any material is responsible for stress concentration around the cavity, making that cross section weaker. In addition, statistical analysis shows that the maximum tensile stress values of embedded specimens (Copper tape Mdn=5.048 MPa & Shape converter embed Mdn=4.976 MPa) are significantly lower than that of specimens with no process interruption (Mdn=12.917MPa), U=0, p=0.05. This difference is higher than the difference observed between process interruption and no process interruption in Section 3.

The Mann-Whitney U test also indicated that the ultimate tensile strength for specimens with only copper tape embed (Mdn= 5.121 MPa) and for specimens with shape converter (Mdn= 4.976 MPa) have no statistically significant difference, U= 4, p=0.827. While the authors hypothesized that shape converters would provide increased adhesion between the last layer before embedding and the resumed layer, there was no improvement in the strength of the parts.

The location of failure for the embedded specimen (Figure 10) was same as that for process interruption seen earlier. All the specimens with any form of process interruption failed at the layer which was paused. Though the two types of embedded specimens had two different depths of cavities (0.5mm for copper tape embed and 3mm for shape converter embed), the failure only occurred at the layer paused. This is an important informatrion for making design decisions; the location of the embed in the design of a loaded part becomes crucial because of these two factors.

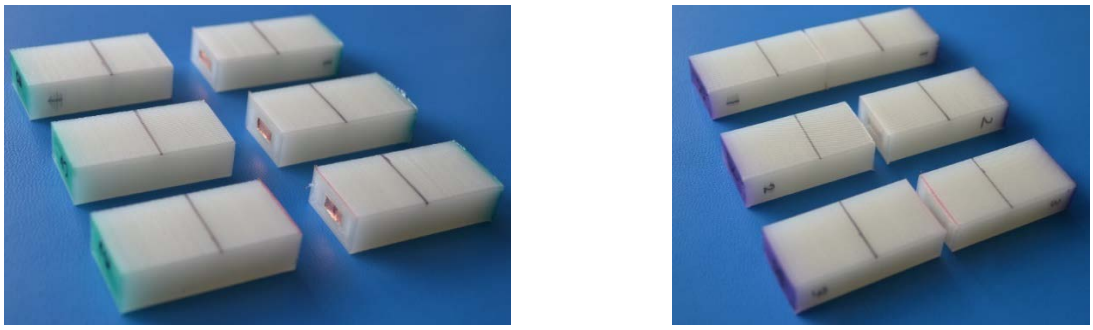

(a) (b)

Figure 10. After tensile testing, (a) copper tape and (b) shape converter embedding specimens with demonstrated failure at the pause layer

4.3 Summary of Key Findings

Tensile testing specimens created to study the effects of embedding helped the authors to conclude the following:

- The presence of an embed causes a significant decrease in Maximum Tensile Stress value compared to that with no process interruption. The median stress value reduced to as low as 38% because of the embed.
- The presence of embed causes a significant decrease in Maximum Tensile Stress value compared to that with only process interruption. A reduction to 70% of the median stress value was observed.
- The presence of a shape converter has no significant effect on tensile properties as compared to an embed without shape converters.
- The weakness is introduced on the layer which is paused, regardless of the embedding process, and the depth of the embedding cavity.

It can be assumed that the process of embedding significantly reduces the strength of the part because of two factors; process interruption and presence of a cavity for embedding. Although one might assume that the use of a shape converter for embedding should assist in improving the adhesion between the layers paused and resumed for embedding, the experiment demonstrated that this is not the case.

5. CLOSURE AND FUTURE WORK

For AM embedding applications to effectively produce end-use functional products, design for AM is crucial. Design for AM involves physical design considerations for components to be embedded, deeper understanding of manufacturing process and its effects on the strength of the part. Knowing how and where a process weakens a part is important information for decision-making while designing. This paper investigated two major steps of an embedding process via material extrusion and their impact on part strength; process interruption and embedding with and without the use of a shape converter. It was found that the process interruption introduces a weakness at the layer of pause and reduces the tensile strength of the part, irrespective of the time duration of pause ≥ 5 minutes. The presence of a shape converter while embedding had no impact on the strength of the part compared to embedding without a shape converter. However, the embedding process reduced the strength of the part compared to that with just process interruption.

A weakness was introduced on the layer paused, regardless of the depth of cavity used for embedding, which resulted in a consistent failure location. This research work provides first known investigation of mechanical influences of process interruption and embedding process on parts made with material extrusion.

These findings provides a wide scope for future work on other in-situ embedding factors, such as the effects of shape converters with different cross sectional areas. A larger set of data for investigating the impact of process interruption with respect to time duration of pause can help in better understanding of abnormality observed in the statistical analysis. Also, this investigation was done for pause time durations varying from 5 minutes to 60 minutes. An investigation of shorter time durations of process interruption than 5 minutes might show an impact on strength of the part. Future work will aim to expand on the impact of material transition on strength when the print is resumed. A range of material will be investigated for layer adhesion while embedding, so as to provide a database of information about their influences on strength. A range of other process types under AM will also be compared for the influence of embedding on mechanical properties of the parts. This can aid in making better decisions for material and process selection while designing.

6. REFERENCES

[1] Campbell, I., Bourell, D., and Gibson, I., 2012, "Additive manufacturing: rapid prototyping comes of age," Rapid Prototyp. J., **18**(4), pp. 255–258.

[2] Bellini, A., Güçeri, S., and Bertoldi, M., 2004, "Liquefier Dynamics in Fused Deposition," J. Manuf. Sci. Eng., **126**(2), p. 237.

[3] Kumar, V., Rajagopalan, S., Cutkosky, M. R., and Dutta, D., 1998, "Representation and Processing of Heterogeneous Objects for Solid Freeform Fabrication," Geom. Model. Work., pp. 1–21.

[4] Meisel, N. A., Elliott, A. M., and Williams, C. B., 2015, "A procedure for creating actuated joints via embedding shape memory alloys in PolyJet 3D printing," J. Intell. Mater. Syst. Struct., **26**(12), pp. 1498–1512.

[5] MarkForged, (2015) MarkForged, Mechanical Properties.

[6] Sterling, B., 2005, SHAPING THINGS, MEDIAWORK, The MIT Press, London, England.

[7] MacDonald, E., Salas, R., Espalin, D., Perez, M., Aguilera, E., Muse, D., and Wicker, R. B., 2014, "3D printing for the rapid prototyping of structural electronics," IEEE Access, **2**, pp. 234–242.

[8] Aguilera, E., Ramos, J., Espalin, D., Cedillos, F., Muse, D., Wicker, R., and MacDonald, E., 2013, "3D Printing of Electro Mechanical Systems," Proc. 24th Solid Free. Fabr. Symp., pp. 950–961.

[9] Perez, K. B., and Williams, C. B., 2013, "Combining Additive Manufacturing and Direct Write for Integrated Electronics – A Review," Int. Solid Free. Fabr. Symp. Proc., pp. 962–979.

[10] Gao, W., Zhang, Y., Nazzetta, D. C., Ramani, K., Cipra, R. J., and Lafayette, W., 2015, "RevoMaker : Enabling Multi-directional and Functionally-embedded 3D Printing using a Rotational Cuboidal Platform," Proc. 28th Annu. ACM Symp. User Interface Softw. Technol. - UIST '15, pp. 437–446.

[11] Kortuem, G., Kawsar, F., Fitton, D., and Sundramoorthy, V., 2010, “Smart objects as building blocks for the Internet of things,” Internet Comput. IEEE, **14**(1), pp. 44–51.
[12] Huebler, A. C., Doetz, F., Kempa, H., Katz, H. E., Bartzsch, M., and Brandt, N., 2007, “Ring oscillator fabricated completely by means of mass-printing technologies,” **8**, pp. 480–486.
[13] Isanaka, P., and Liou, F., 2012, “The Applications of Additive Manufacturing Technologies in Cyber Enabled Manufacturing Systems,” Proc. Annu. Int. Solid Free. Fabr. Symp. - An Addit. Manuf. Conf., pp. 341–353.
[14] Espalin, D., Muse, D. W., MacDonald, E., and Wicker, R. B., 2014, “3D Printing multifunctionality: Structures with electronics,” Int. J. Adv. Manuf. Technol., **72**(5-8), pp. 963–978.
[15] Ihn, J., and Chang, F., 2008, Structural Health Monitoring.
[16] Strantza, M., Aggelis, D. G., de Baere, D., Guillaume, P., and van Hemelrijck, D., 2015, “Evaluation of SHM system produced by additive manufacturing via acoustic emission and other NDT methods,” Sensors (Switzerland), **15**(10), pp. 26709–26725.
[17] Kataria, A., Rosen, D. W., Kataria, A., and Rosen, D. W., 2001, “Building around inserts: methods for fabricating complex devices in stereolithography,” Rapid Prototyp. J., **7**(5), pp. 253–262.
[18] Tröger, C., Bens, A. T., Bermes, G., Klemmer, R., Lenz, J., and Irsen, S., 2008, “Ageing of acrylate-based resins for stereolithography: thermal and humidity ageing studies,” Rapid Prototyp. J., **14**(5), pp. 305–317.
[19] Hahnlen, R., and Dapino, M. J., 2010, “Active Metal-matrix Composites with Embedded Smart Materials by Ultrasonic Additive Manufacturing,” SPIE Smart Structures and Materials+ Nondestructive Evaluation and Health Monitoring, pp. 1–12.
[20] Rodriguez, E., Mireles, J., Terrazas, C. A., Espalin, D., Perez, M. A., and Wicker, R. B., 2015, “Approximation of absolute surface temperature measurements of powder bed fusion additive manufacturing technology using in situ infrared thermography,” Addit. Manuf., **5**, pp. 31–39.
[21] Yang, J., Sun, S., Brandt, M., and Yan, W., 2010, “Experimental investigation and 3D finite element prediction of the heat affected zone during laser assisted machining of Ti6Al4V alloy,” J. Mater. Process. Technol., **210**(15), pp. 2215–2222.
[22] Schick, D., Hahnlen, R., and Dehoff, R., 2010, “Microstructural Characterization of Bonding Interfaces in Aluminum 3003 Blocks Fabricated by Ultrasonic Additive Manufacturing,” Welding Journal, **89**, pp. 105-115.
[23] Truog, A. G., 2012, “Bond improvement of Al/Cu joints created by very high power ultrasonic additive manufacturing.”
[24] Cham, J., Pruitt, B., Cutkosky, M. R., Binnard, M., Weiss, L. E., and Neplotnik, G., 1999, “Layered manufacturing with embedded components: process planning considerations,” Proc. DETC99 1999 ASME Des. Eng. Tech. Conf., pp. 1–9.
[25] Sbriglia, L. R., Baker, A. M., Thompson, J. M., Morgan, R. V, Wachtor, A. J., and Bernardin, J. D., 2016, “Embedding Sensors in FDM Plastic Parts During Additive Manufacturing,” **10**, pp. 205–214.
[26] Stark, B., Stevenson, B., Stow-Parker, K., and Chen, Y., 2014, “Embedded sensors for the health monitoring of 3D printed unmanned aerial systems,” 2014 Int. Conf. Unmanned Aircr. Syst. ICUAS 2014 - Conf. Proc., pp. 175–180.

[27] Aguilera, E., Ramos, J., Espalin, D., Cedillos, F., Muse, D., Wicker, R., and MacDonald, E., 2013, “3D printing of electro mechanical systems,” 24th Int. SFF Symp. - An Addit. Manuf. Conf., pp. 950–961.
[28] Sood, A. K., Ohdar, R. K., and Mahapatra, S. S., 2010, “Parametric appraisal of mechanical property of fused deposition modelling processed parts,” Mater. Des., **31**(1), pp. 287–295.
[29] Klift, F. Van Der, Koga, Y., Todoroki, A., Ueda, M., and Hirano, Y., 2016, “3D Printing of Continuous Carbon Fibre Reinforced Thermo-Plastic (CFRTP) Tensile Test Specimens,” Open Journal of Composite Materials, pp. 18–27.
[30] Dumstorff, G., and Lang, W., 2014, “Failure of Silicon Substrates Embedded in Epoxy Resin,” Procedia Technol., **15**(0), pp. 216–220.
[31] ASTM Norma, 2004, “Standard Test Method for Tensile Properties of Plastics,” Annu. B. ASTM Stand., pp. 1–15.
[32] Jaksic, N. I., 2015, “What to do when 3D printers go wrong: Laboratory experiences,” 122nd ASEE Annu. Conf. Expo.